AGU PUBLICATIONS

JGR

Journal of Geophysical Research: Biogeosciences

RESEARCH ARTICLE
10.1002/2015JG003014

Key Points:
- Coastal vegetation pattern and primary production will be modified following environmental stress
- The competitive advantage of exotic species was weakened due to lower tolerance when under stress
- The resilience of native species that adapted to changed geophysical features was to be expected

Supporting Information:
- Supporting Information S1

Correspondence to:
Z.-M. Ge,
zmge@sklec.ecnu.edu.cn

Citation:
Ge, Z.-M., H.-B. Cao, L.-F. Cui, B. Zhao, and L.-Q. Zhang (2015), Future vegetation patterns and primary production in the coastal wetlands of East China under sea level rise, sediment reduction, and saltwater intrusion, *J. Geophys. Res. Biogeosci.*, *120*, 1923–1940, doi:10.1002/2015JG003014.

Received 8 APR 2015
Accepted 9 SEP 2015
Accepted article online 14 SEP 2015
Published online 9 OCT 2015

Future vegetation patterns and primary production in the coastal wetlands of East China under sea level rise, sediment reduction, and saltwater intrusion

Zhen-Ming Ge[1,2], Hao-Bin Cao[1], Li-Fang Cui[1], Bin Zhao[3], and Li-Quan Zhang[1]

[1]State Key Laboratory of Estuarine and Coastal Research, East China Normal University, Shanghai, China, [2]School of Forest Sciences, University of Eastern Finland, Joensuu, Finland, [3]Ministry of Education Key Laboratory for Biodiversity Science and Ecological Engineering, School of Life Sciences, Fudan University, Shanghai, China

Abstract To explore the effects of sea level rise (SLR), sediment reduction (SR), and saltwater intrusion (SWI) on the vegetation patterns and primary production of one exotic (*Spartina alterniflora*) and two native dominant (*Scirpus mariqueter* and *Phragmites australis*) species in the coastal wetlands of East China, range expansion monitoring and stress experiments were conducted, followed by model prediction. After a rapid invasion period, the expansion rate of *S. alterniflora* slowed down due to the decreasing availability of suitable habitat under prolonged inundation. SLR was shown to decrease the colonization of *S. alterniflora* and the native *P. australis* up to 2100. In contrast, the native *S. mariqueter* that has a high tolerance of inundation increased in area following SLR, due to a reduction in competition from *S. alterniflora* in low-lying habitats and even recolonized areas previously invaded by the exotic species. The combination of SLR and SR resulted in further degradation of *S. alterniflora* and *P. australis*, while the area of *S. mariqueter* was not reduced significantly. The decrease in the area of vegetation would reduce the gross primary production under SLR and SR. SWI exacerbates the impacts, especially for *P. australis*, because *S. alterniflora* and *S. mariqueter* have a higher tolerance of salinity. Thus, the coastal vegetation pattern was predicted to be modified due to species-specific adaption to changed geophysical features. This study indicated that the native species better adapted to prolonged inundation and increased salinity might once again become key contributors to primary production on the muddy coasts of East China.

1. Introduction

The combined influence of climate change and plant invasions on ecosystems has recently become a matter of serious concern [*Bradley et al.*, 2009; *Scott et al.*, 2010; *Sheppard et al.*, 2014]. However, responses of the coastal wetlands comprising both exotic and native species to predicted environmental change have received scant attention [*Mendoza-González et al.*, 2013; *Seabloom et al.*, 2013]. The long-term stability of coastal wetlands is a function of interactions between sea level and sediment deposition that ultimately regulate the equilibrium between the elevation of mudflats and the prevailing sea level [*Morris et al.*, 2002; *Mudd et al.*, 2009]. Consequently, climate change is hypothesized as leading to large-scale range shifts in vegetation patterns, mainly through the acceleration of sea level rise (SLR) and associated changes in sedimentation processes.

Based on the fifth assessment report (AR5) by the Intergovernmental Panel on Climate Change (IPCC) [*Church et al.*, 2013], the rate of global mean SLR (44–74 cm) by 2100 is attributed to increases in ocean warming and the loss of mass from glaciers and ice sheets. According to the latest bulletin released by the State Oceanic Administration *State Oceanic Administration People's Republic of China (SOA)*, 2013], China's coastal sea level rose by an average rate of 2.9 mm yr^{-1} over the period of 1980–2013, which is faster than the global average (see Figure 1). Due to dramatic increases in the rate of seawall construction, Chinese coastal zones with low elevations have been identified as particularly vulnerable to the expected SLR [*SOA*, 2013; *Ma et al.*, 2014]. Variations in salinity represent another severe consequence of SLR. Many studies have indicated that SLR has a pronounced effect on saltwater intrusion (SWI) in estuarine and coastal zones, as has been demonstrated in cases from the Georgia and South Carolina coasts in the U.S. [*Conrads et al.*, 2013] and the Yangtze Estuary and Pearl River Estuary in China [*Qiu and Zhu*, 2015; *Yuan et al.*, 2015].

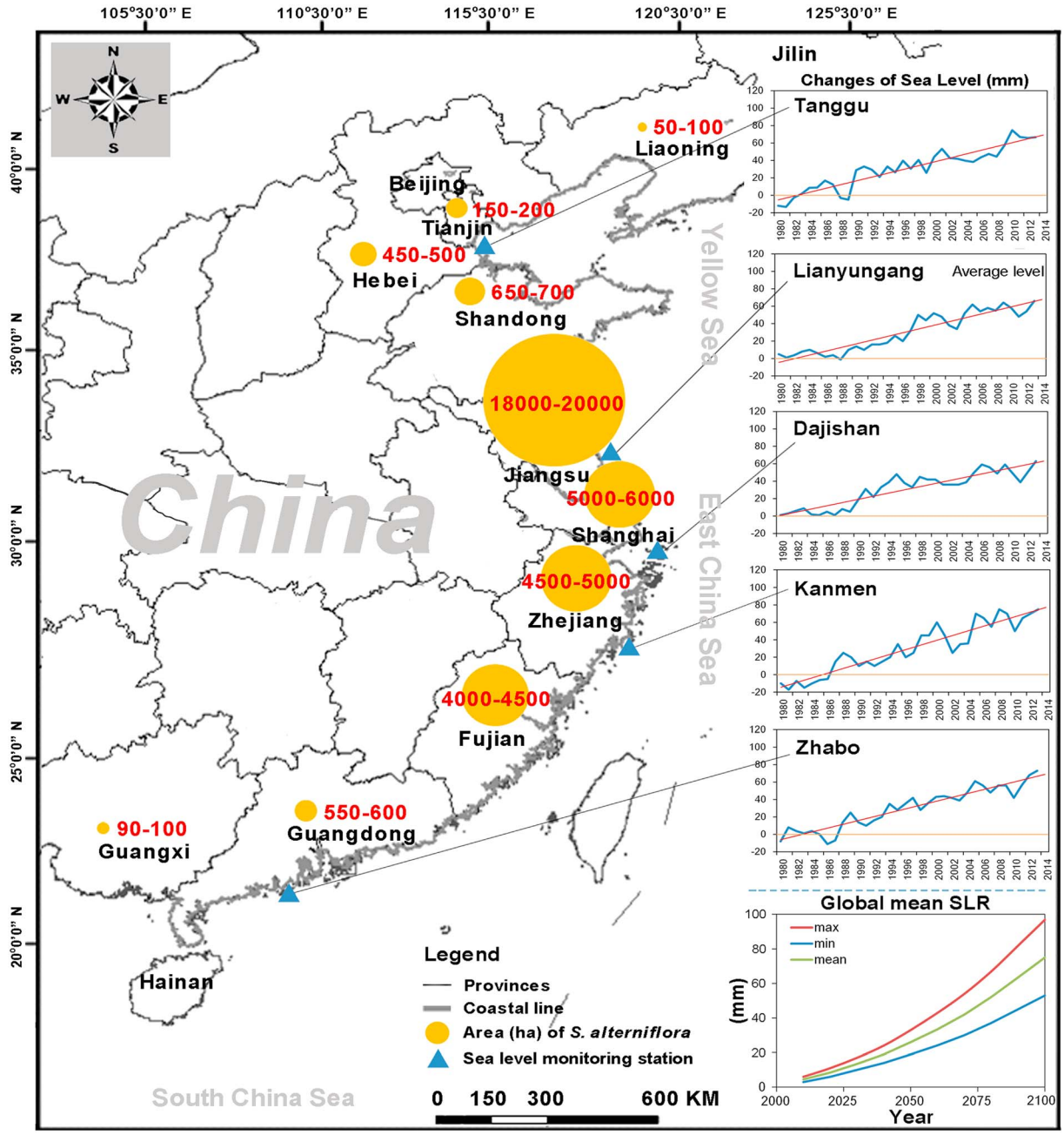

Figure 1. Mean change in sea level along China's coastline (documented in 2013 by *SOA* [2013]) and *S. alterniflora* invasion in the coastal wetlands (documented in 2007).

For the muddy coasts with a high sediment loading in China, sediment deposition in coastal wetlands increases land elevation and the area of salt marshes, favoring the propagation and expansion of macrophytes [*Guan*, 2012]. However, the construction of the Three Gorges Dam (TGD) upstream on the Yangtze River has exerted a significant impact on both the hydrological and geomorphologic settings of both the river and the downstream estuary. The sediment discharge at Datong station, in the Yangtze River, fell from ~490 megaton (Mt) yr^{-1} in the 1950s and 1960s to ~150 Mt yr^{-1} after the closure of the TGD in 2003 [*Yang et al.*, 2011]. In the Yangtze Estuary, this dramatic reduction in the sedimentation rate (SR) has further exacerbated the impacts of SLR and caused the loss of coastal wetlands and degradation of the salt marsh vegetation [*Yang et al.*, 2005].

Spartina alterniflora, which was introduced to China from North America in the late 1970s initially for ecological engineering purposes, has been expanding rapidly along China's coastline [*Guan*, 2012] (see Figure 1).

As documented in 2008 in the Yangtze Estuary, the area occupied by *S. alterniflora* accounted for approximately 30% of the total intertidal salt marsh vegetation [*Chen et al*., 2008; *Li et al*., 2009; *Zhou and Xie*, 2012]. During the last decade in the Yangtze Estuary, the vegetation in coastal wetlands has been studied extensively in terms of the spatiotemporal dynamics of plant invasion [*Li et al*., 2009; *Xiao et al*., 2010; *Ge et al*., 2015a], adverse effects of exotic species on native habitats and biodiversity [*Chen et al*., 2004; *Wang et al*., 2006; *Ma et al*., 2011], seed characteristics and the seed bank [*Xiao et al*., 2009], plant physiology [*Jiang et al*., 2009; *Ge et al*., 2014], and interactions between the vegetation and hydrodynamic regimes [*Schwarz et al*., 2011]. Based on the results of previous studies, a detailed model of vegetation pattern was developed to aid in the understanding of the biotic and abiotic factors that regulate the spatiotemporal dynamics of the coastal vegetation communities including exotic *S. alterniflora* (Poaceae) and dominant native species of *Scirpus mariqueter* (Cyperaceae) and *Phragmites australis* (Poaceae) [*Ge et al*., 2013, 2015a]. At the same time, a process-based primary production model was developed in combination with the vegetation pattern model for exotic and native plants in relation to their biochemical properties, leaf-to-canopy characteristics, and plant phenology [*Ge et al*., 2015b].

In this study, the potential response of vegetation in coastal wetlands of East China to the interactive disturbances of SLR, SR, and SWI was explored, and the balance between exotic and dominant native species was highlighted. First, the range expansion of exotic and native species was compared based on 3 years of monitoring within sample areas with varying geographical and hydrological features. Then, the tolerance of vegetation to inundation duration and the resulting changes in primary production under high salinity were tested using environmental restriction experiments to parameterize the coupled model. Finally, an analysis of the impact of environmental change on the pattern of vegetation and primary production was carried out by applying the model under current and changed conditions. The following questions were addressed: (1) would the invasive species colonize the coastal wetlands at the same rate as occurred in the previous decade? (2) Would the future vegetation pattern be modified due to a species-specific expansion mode and tolerance to inundation under SLR and SR? And (3) would primary production over the study area be regulated by the interactive effects of SLR, SR, and SWI?

2. Material and Methods

2.1. Study Area

The effects of SLR, SR, and SWI on vegetation pattern and primary production in the coastal wetlands were tested by setting up a series of field monitoring and stress experiments in the Yangtze Estuary. The study area was located on the two largest coastal wetlands, named the Chongming Dongtan wetland (hereafter CDW) and the Jiuduansha wetland (hereafter JW) in the estuary (Figure 2). CDW (31°25′–31°38′N, 121°50′–122°05′E) is located on the eastern fringe of Chongming Island with an area of 242 km^2 above the 0 m isobaths. Closing to CDW, JW (31°03′–3°17′N, 121°46′–122°15′E) is an isolated shoal with an area of 127 km^2. Tidal movement in the estuary is irregular and semidiurnal, with maximum and average tide heights of 4.62–5.95 m and 1.96–3.08 m, respectively, based on the local Wusong bathymetric benchmark [*Ge et al*., 2008]. The estuary has an eastern Asian monsoon climate with an average annual temperature from 15.2 to 15.8°C. The average annual precipitation is approximately 1022 mm and the average humidity 82%.

S. alterniflora was first introduced to the coastal wetlands in the Yangtze Estuary in the 1990s, and this exotic species has gradually invaded large areas of unvegetated mudflats and has also begun to invade the area that was formerly covered by native vegetation [*Li et al*., 2009; *Ge et al*., 2013]. By 2012, the total area of *S. alterniflora* that had been invaded was more than 6200 ha [*Ge et al*., 2015a]. The increase in the area of *S. alterniflora* was approximately 1500 ha and 2100 ha on CDW and JW, respectively. In contrast, the area of native *S. mariqueter* declined by 30% and 42% on CDW and JW between 2003 and 2012, respectively [*Zhou and Xie*, 2012].

2.2. Survey and Experiment Design

2.2.1. Range Expansion of Exotic and Native Species

During the survey period from 2008 to 2010, the expansion of *S. alterniflora* in the two habitats with high (~3.0 m) and low (~2.5 m) elevation was monitored regularly in the marsh frontiers on the CDW. In the low-lying habitat, the expansion rate of *S. mariqueter* was also investigated. Three fixed transects (5 m in width) were set up running perpendicularly from the fringe of the meadow seaward to the bare mudflat

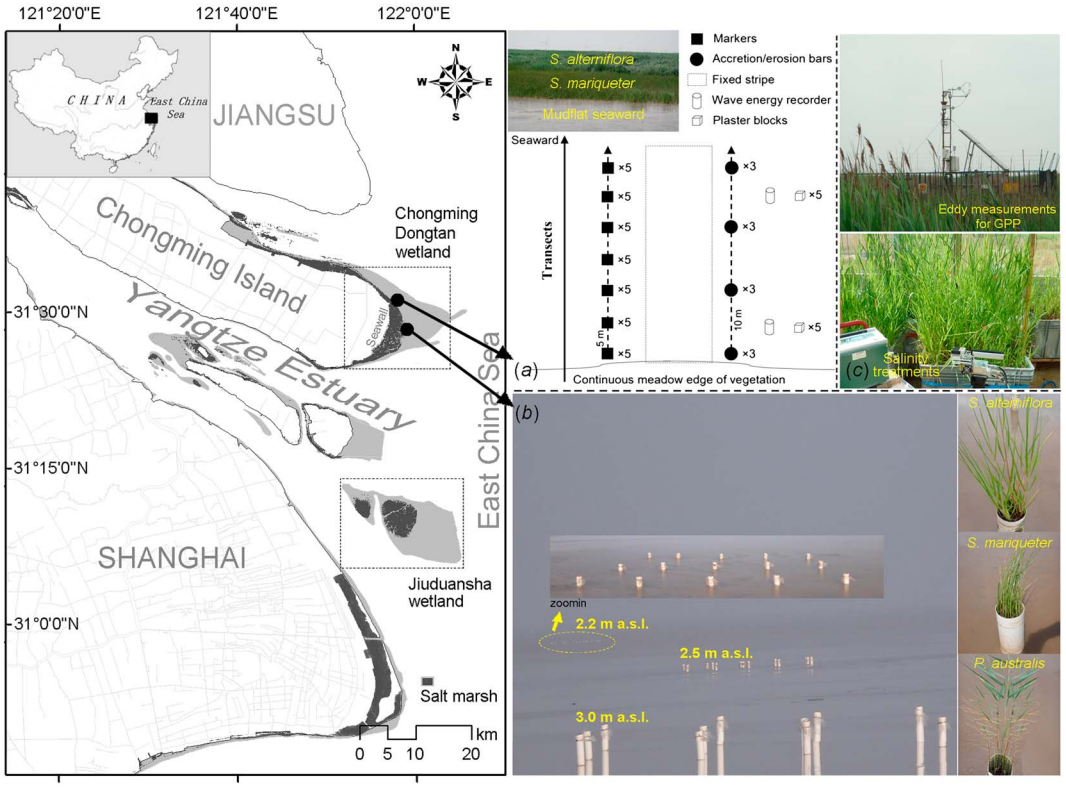

Figure 2. Location of the Chongming Dongtan wetland (CDW) and Jiuduansha wetland (JW) in the Yangtze Estuary, with the experimental setup of (a) the monitoring strips for the expansion of *S. alterniflora* and *S. mariqueter* along the mudflat front and the measurement of accretion/erosion regimes; (b) the determination of a tolerance limits of plant survival under inundation stress with mesocosms of *S. alterniflora*, *S. mariqueter*, and *P. australis*; and (c) the investigation of the photosynthesis and growth of plants under salinity stress with mesocosms of *S. alterniflora*, *S. mariqueter*, and *P. australis*.

(Figure 2a). Bamboo markers were placed at 5 m intervals along each transect to quantify the expansion rate of vegetation by bimonthly recording of the distance between markers and the fringe of meadow. The spatial colonization (>50% coverage) of *S. alterniflora* and *S. mariqueter* along transects was also mapped with a resolution of 1 m × 1 m bimonthly from March to November during 2008–2010 to record the dynamics of vegetation pattern on the two types of marsh. The expansion rate of *P. australis* was much slower than that of *S. alterniflora*, and most of the distribution area was located on the high-elevation mudflat [*Ge et al.*, 2015a].

Based on previous surveys [*Xiao et al.*, 2010; *Schwarz et al.*, 2011], the range expansion of vegetation was shown to occur through seedling establishment, tussock development, and sediment accretion. Therefore, both biotic and abiotic factors were measured (data not presented in this paper but used for model parameterization; see supporting information).

2.2.2. Tolerance of the Vegetation to Changes in Duration of Inundation

To test the tolerance of the vegetation to the increased inundation duration following SLR, three platforms containing mesocosms of *S. alterniflora*, *S. mariqueter*, and *P. australis* were constructed at different elevations (Figure 2b) to simulate the response of plant survival to different flooding regimes. The mesocosms were grown on the open tidal flat over an entire growing season. Therefore, this experiment provided a direct assessment of the species-specific response of plant growth to changes in the relative elevation.

Each platform contained 30 mesocosms that were composed of a 16 cm diameter (200 cm^2) PVC pipe for *S. alterniflora*, *S. mariqueter*, and *P. australis*, with 10 replicates of each. In March 2013, intact soil monoliths (50 cm depth) consisting of vegetation seedlings were cored with PVC pipes from the CDW. The plant materials were collected at the same tidal line and had seedlings with similar life forms. The pipes with mesocosms were buried 50–80 cm into the mudflat substrate and three elevation levels (3.0 m, 2.5 m, and 2.2 m, Figure 2b) of the soil surface in the pipes were obtained. The elevation of the mesocosms was determined using a Real-Time Kinematic Global Position System (Ashtech, USA), and the double-rods method was

employed to determine the bed-level changes on the CDW following the practice of *Yang et al*. [2005]. The rims of the pipes were sawn to allow water leakage, avoiding waterlogging in the pipes during the low-tide phase.

Taking the number of living seedlings before the experiment as the initial density, the changes in the survival rate of plants were recorded monthly over the growing season. The information on the tidal regimes in the Yangtze Estuary was obtained from real-time monitoring and the official annals of the Shanghai Water Authority and the Shanghai Municipal Ocean Bureau.

To build the relationship between plant survival and inundation duration (reflected by relative elevation), a simple elevation-based logistic function was used to explore the tipping points of the species to inundation duration.

$$f(E) = \frac{1}{1 + \exp\left[\frac{-(E-a)}{k}\right]} \tag{1}$$

where E is the mudflat elevation a and k are the fitting parameters.

In general, the downregulated curve of the logistic probability law constitutes three meaningful phases: the start of decline, steep decline, and an irretrievable point. This third point was taken to reflect the tipping point (P) of plant survival to the inundation duration with a hypothesis (H) of maximum entropy.

$$\text{Max } H(P) = \left(f^2(E+i) - f^2(E)\right) - \left(f(E+i) - f(E)\right) \tag{2}$$

where P is identified when the maximum of the function was obtained and i is the regular sample unit of elevation.

2.2.3. Photosynthesis and Growth Under Salinity Stress

Based on a pilot study, salinity stress was shown not to increase the mortality of vegetation, while it significantly influenced the photosynthetic performance and the consequent primary production of plants. In March 2013, the mesocosms consisting of *S. alterniflora*, *S. mariqueter*, and *P. australis* seedlings with intact soil monoliths (0.5 m × 0.5 m × 0.5 m) were sampled from the CDW. The mesocosms were grown in high-density polyethylene containers for the salinity stress experiment (Figure 2c). Before experimental treatments, the plants were maintained for 30 days with freshwater and allowed to recover from being transplanted in the greenhouse chamber. A total of 36 containers (three species × three salinity treatments × four repetitions) with vegetation were treated with three levels of salinity, ranging from 0‰ (freshwater) to 15‰ (moderate salinity) and 30‰ (high salinity). During the pretreatment period, the salinity levels were increased by 5‰ and 10‰ per week, until the flooding treatments reached the experimental salinity levels, and the water was replaced weekly.

During the period from May to October, measurements of maximum net photosynthetic rate (P_{max}, 25°C) were conducted monthly with a portable steady state photosynthesis system (Li-Cor 6400, Li-Cor Inc., Lincoln, NE, USA), following *Ge et al*. [2014]. In July, the net photosynthetic rate (P_n) with stomatal conductance was measured at a leaf temperature range from 15 to 35°C with intervals of 5°C. After the gas exchange measurement, the biomass of the plants was determined by weighing the annual increment of aboveground and belowground dry mass, as outlined in *Ge et al*. [2012].

2.3. Model Framework

2.3.1. Vegetation Pattern

A salt marsh model for the Yangtze Estuary (SMM-YE) was constructed on the basis of the dynamics of vegetation pattern in the coastal wetlands (Figure 3). Based on the measurements and experiments, the biotic processes of the seed bank and germination, duration of the growing period, reproduction and establishment, clonal integration and tolerance to inundation stress (mortality), as well as interspecies competition between the exotic and native species, were parameterized and validated [*Ge et al*., 2013, 2015a].

The vegetation pattern model was constructed using the MATLAB® matrix platform. The habitat pattern map consists of a spatial lattice of interconnected cells, which were connected to all neighboring cells with a distribution probability for the vegetation. Habitat cells indicating open water, bare mudflat, and native species (*S. mariqueter* and *P. australis*) and exotic species (*S. alterniflora*) were coded. As the model runs, each cell evolves according to the transition rules, which depend on the state of its neighboring cells. In order to estimate spatially the vertical elevation changes at each cell, the model superimposes the geographic matrix

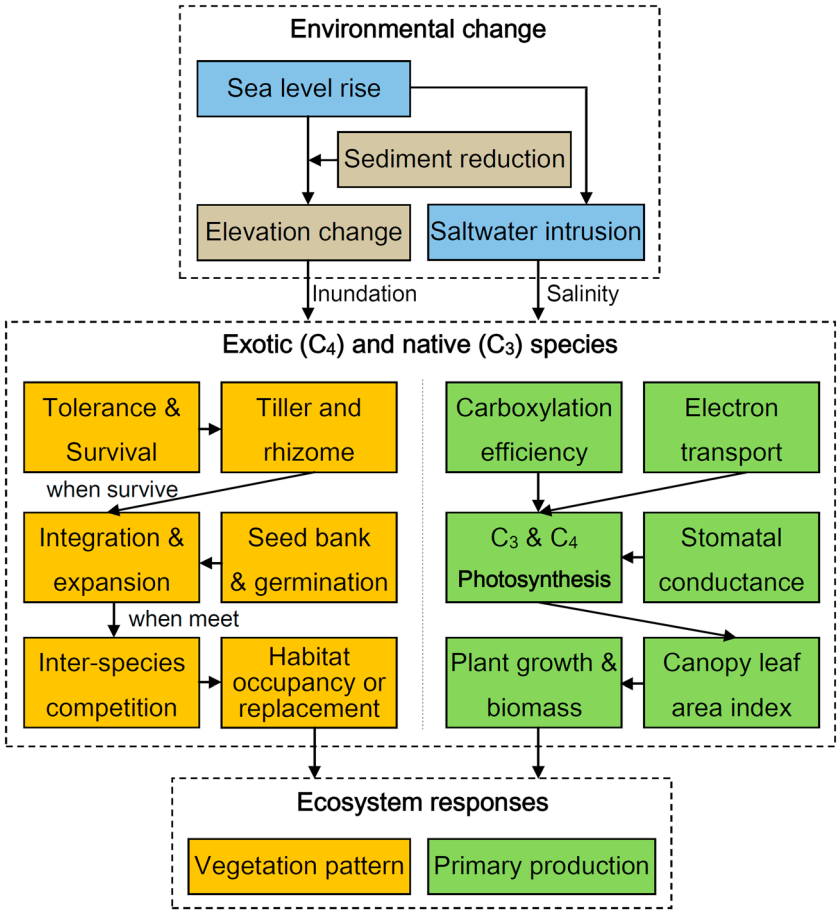

Figure 3. Model framework for estimating the effects of SLR, SR, and SWI on vegetation pattern and primary production in the coastal wetlands.

onto the annual mean rate of sedimentation regime on the initial digital elevation map to renew the mudflat elevation on the elevation matrix and the subsequent increase in lateral mudflat area. The model was further designed to quantify the abilities of the three dominant species to trap suspended sediment for vertical accretion. The detailed information on the model structure and parameterization is summarized in the supporting information.

2.3.2. Primary Production

To understand the spatiotemporal variations in primary production in conjunction with community dynamics, a process-based production model, based on the biochemical properties, canopy characteristics, and plant phenology of the exotic and native species [*Ge et al*., 2015b], was incorporated into the vegetation pattern model (Figure 3). This biochemical model is reasonably capable of simulating the photosynthetic performance of C_3 and C_4 species growing under different environmental conditions, for instance, salinity [*Ge et al*., 2014].

For the exotic and native species, the production model for gross primary production (GPP) estimation was based on the species-specific photosynthesis. The modeled seasonal fluxes and annual amount of GPP in both exotic (C_4 plants) and native species (C_3 plants) had been validated against the eddy covariance measurements (Figure 2c) over a 4 year period [*Ge et al*., 2015b]. The physiological core of the model lies in the biochemical functions of leaf photosynthesis as developed for C_3 [*Farquhar et al*., 2001] and C_4 plants [*von Caemmerer and Furbank*, 1999]. To simulate the whole seasonal variability of GPP and NPP, the phenological properties and seasonal course of leaf area index development of *S. alterniflora*, *S. mariqueter*, and *P. australis* were embedded into the photosynthesis calculations. The detailed algorithms for leaf-to-canopy processes are presented in the supporting information.

Table 1. Scenarios for the Model Simulation

Item	Scenario	
	Current	Changed
SLR	none	74 cm increase by 2100[a]
SR	CSR	−1/4 CSR[b]
SWI	~3‰ of salinity	10‰ salinity by 2100[c,d]

[a]Median values of IPCC RCP 8.5 [*Church et al*., 2013].
[b]25% decrease in current sedimentation rate (CSR; see supporting information).
[c]*Kong et al*. [2004].
[d]*Qiu and Zhu* [2015].

2.4. Scenario Analysis

2.4.1. Initial Database for Model

The initial digital maps of vegetation pattern from 2008 for the CDW and JW were documented by the national wetlands resource investigation and monitoring program [*Zhou and Xie*, 2012]. In the model, the MATLAB matrix platform for each distribution polygon of vegetation was produced for projection.

A digital elevation model of the Yangtze Estuary was constructed with the remotely sensed data of 2008, using the Krasovsky 1940 transverse Mercator coordinate system and the transverse Mercator map projection [*Wang et al*., 2014]. The isobath information was provided by the nautical charts of the Yangtze Estuary from the Chinese Navy. Using ArcGIS 10.0, the mean tidal level, isobaths of 0 m, −2 m, and −5 m were delineated, based on the local Wusong bathymetric benchmark.

A digital map with sedimentary data was produced to comply with the input requirements of the model. Data on the sedimentation rate (mean value from 1997 to 2010) from the Survey Bureau of Hydrology and Water Resources of the Changjiang River Estuary (documented by the Changjiang Water Resources Commission [*Changjiang Water Resources Commission*, 2012]) were used. The observation data were obtained over the survey period at Waigaoqiao tidal gauge station and are based on the local Wusong bathymetric benchmark. A data set describing the spatial sedimentation regime covering the Yangtze Estuary for year-to-year mudflat accretion and elevation change was used for the vegetation pattern model (see supporting information).

2.4.2. Scenarios of SLR, SR, and SWI

The model simulations were based on scenario sets (current and changed conditions) of SLR, SR, and SWI (Table 1). Based on the IPCC RCP 8.5 scenario of AR5 [*Church et al*., 2013], the likely ranges of global mean SLR are 52–98 mm by 2100. In the Yangtze Estuary, the regional projection and global average rate adopted for the evaluation was 74 cm by the year 2100 (median values of RCP 8.5 scenario). The current sea level referred to the local Wusong bathymetric benchmark.

Two scenarios of sedimentation rates were also adopted for the simulations. The current sedimentation rate was taken as the mean sedimentation rate for the period 1997–2010. The scenario of SR was taken as three quarters of the current sedimentation rate (Table 1), which could be anticipated as a result of the various engineering projects upstream on the Yangtze River [*Yang et al*., 2011].

As documented by the Shanghai Water Authority and the Shanghai Municipal Ocean Bureau, the seasonal variation of salinity in the study area ranged from 0.6 to 10.5‰ with a mean value of ~3‰ during the growing season. As predicted by *Qiu and Zhu* [2015], the monthly mean salinity would, on average, increase to 10‰ by 2100 with a SLR scenario of 10 mm yr^{-1}.

2.4.3. Model Simulation

Over the simulation period of 2000–2100, the prediction of future vegetation pattern and primary production was conducted using the current (2000–2100) and changed scenarios (2008–2100) to identify the effects of SLR, SR, and SWI. The same initial inputs were used for scenario analysis, i.e., the geographical data from the classified vegetation pattern, digital elevation map, and sedimentation regime. Due to the presence of stochastic elements and processes in the model [*Ge et al*., 2015a], the calculations were repeated 10 times. During the simulation, the elevation matrix map was overlain on top of the matrix of plant distribution to determine the habitable cells for expansion, survival, and establishment of plants under SLR and SR. Under the scenarios of SLR and SR, the relative elevation (E_R) of habitat will alter, resulting in changes in daily duration of submergence. Based on the field experiments, the model assumed that the plants could not survive when E_R reaches P for different species.

$$ER = E - H_{SLR} - H_{SR} \quad (3)$$

where H_{SLR} and H_{SR} are the changes in elevation resulted from SLR and SR, respectively.

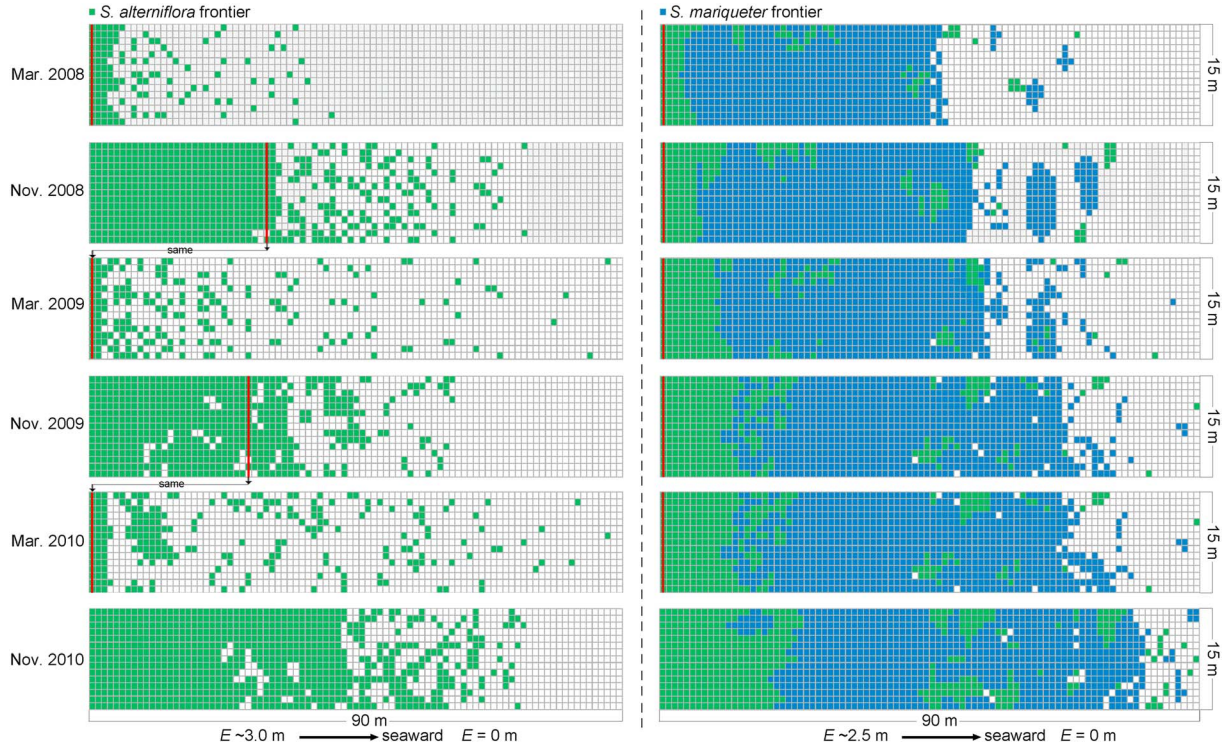

Figure 4. Range expansion of *S. alterniflora* and *S. mariqueter* from March to November during the period 2000–2008. Red lines show the starting points for monitoring in March.

The scenario of SWI (salt water intrusion) was used for evaluating the responses of photosynthesis and the consequent primary production.

$$\text{Parameter}' = \text{Parameter} \times f(\text{salinity}) \quad (4)$$

where *parameter'* is the modified photosynthetic parameters for the native C_3 and exotic C_4 species in terms of the maximum rate of carboxylation by Rubisco, the maximum rate of electron transport, and the maximum rate of PEP carboxylation [*Ge et al.*, 2014], based on the salinity stress experiment (see supporting information).

To calculate the seasonal leaf-to-canopy photosynthesis and GPP, the daily means of meteorological data (air temperature, solar radiation, CO_2 concentration, and relative humidity) documented by the Chongming Meteorological Bureau during 2000–2012 were used repeatedly over the total simulation period.

2.5. Data Analyses

The means of the survival rates under an elevation gradient were fitted with *S* curves (equations (1) and (2)) to estimate the tipping points for inundation duration for *S. alterniflora*, *S. mariqueter*, and *P. australis*. Differences in the photosynthesis and biomass growth of vegetation under salinity treatments were tested using analysis of variance and Tukey's HSD test. Statistical significance was assessed at $p < 0.05$.

The means ($n = 10$ repeated simulations) of the modeled distribution area and primary production of the exotic and native species in the short term (2025), medium term (2050), and long term (2100) were analyzed with paired *t* tests between the current and the changed scenarios. The statistical analyses were performed in SPSS (SPSS 18.0 for Windows, SPSS Ltd., USA).

3. Results

3.1. Species-Specific Colonization at the Marsh Frontier

During the monitoring period, the mean distance of range expansion from the continuous *S. alterniflora* meadow through the growing seasons reached 29.5 ± 4.4 m in 2008, 25.8 ± 2.5 m in 2009, and 39.6 ± 6.5 m in 2010, in the habitat at ~3 m elevation (Figure 4). The seedlings of *S. alterniflora* were transported to the

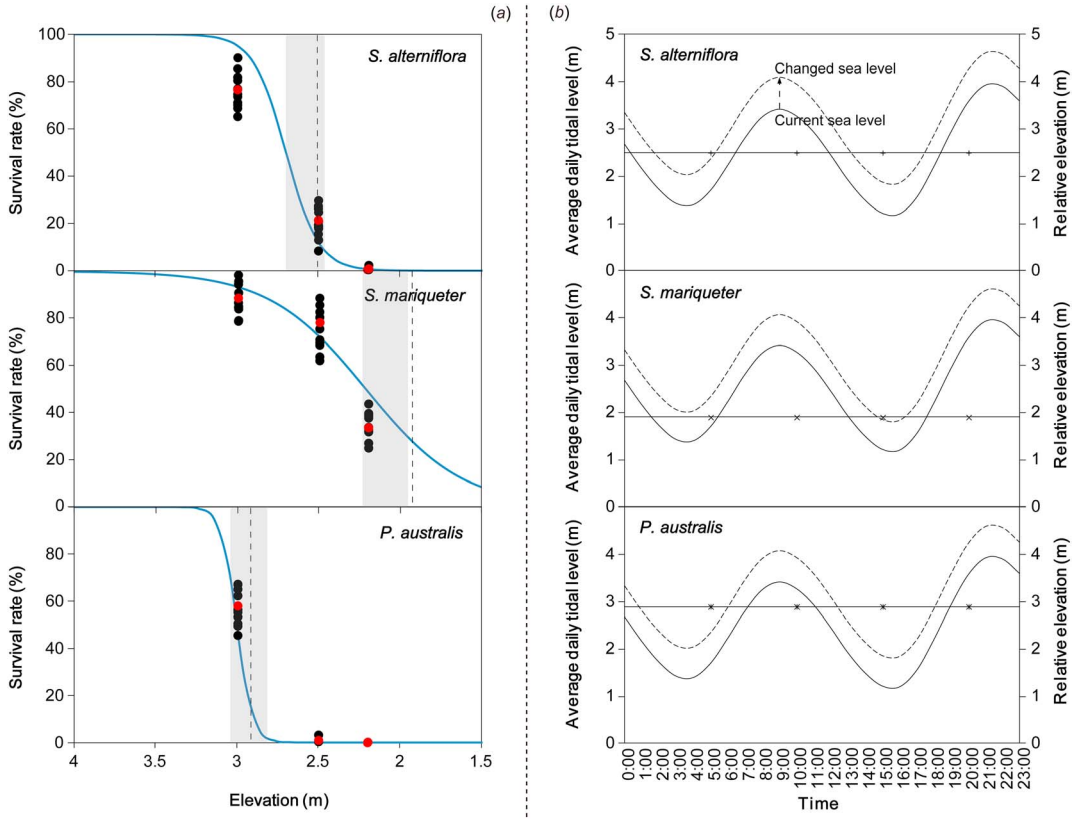

Figure 5. (a) Fitting curves of plant survival (red points are the means) and tolerance limits (dotted line) under inundation treatments (by variations of elevation). Grey area shows the lower boundary of vegetation distribution based on field survey. (b) Mean daily tidal range and inundation duration for *S. alterniflora*, *S. mariqueter*, and *P. australis* under the current and changed sea level.

mudflat seaward by the tidal flow in spring (around March). Then, the seedlings that established on the mudflat grew quickly through asexual propagation and integrated through tillers and rhizomes during the growing season, coalescing into new meadows by the autumn (around October). In the low-lying (~2.5 m) habitat, the expansion rate of *S. alterniflora* (4.2 ± 0.4 m) was significantly ($p < 0.05$) lower than that in the high-elevation habitat (Figure 4). The mean distance of range expansion from the continuous *S. mariqueter* meadow through the growing seasons reached 6.2 ± 1.1 m in 2008, 10.2 ± 7.5 m in 2009, and 8.7 ± 0.8 m in 2010 (Figure 4). The range expansion of *S. mariqueter* occurred mainly from lateral vegetative propagation, and few seeds and seedling banks were found on the mudflats.

3.2. The Limits of Tolerance Under Inundation Stress

Based on the experiments on the tolerance of plants to varying inundation conditions (variations of elevation), the survival curves were fitted in relation to elevation for the salt marsh vegetation (Figure 5a). With the downregulated logistic curve, the habitat elevation that reflected the tolerance threshold (irreversible growth) for inundation duration was identified to be 2.5 m for *S. alterniflora*, 1.9 m for *S. mariqueter*, and 2.9 m for *P. australis*. Across the mean daily tidal range, the threshold of the mean daily inundation duration for *S. alterniflora*, *S. mariqueter*, and *P. australis* was estimated to be approximately 11, 16, and 9 h d^{-1}, respectively (Figure 5b).

3.3. Effects of Salinity Stress on Plants

S. alterniflora exhibited a greater P_{max} (17.5−28.9 μmol m^{-2} s^{-1}) than *S. mariqueter* (10.2−25.0 μmol m^{-2} s^{-1}) and *P. australis* (11.6−23.1 μmol m^{-2} s^{-1}) through the growing season (Figures 6a–6c). The limitation of P_{max} in *S. alterniflora* and *S. mariqueter* was marginal under the 15‰ salinity treatment, except at the latter stage, while it led to a significant ($p < 0.05$) decrease in P_{max} in *P. australis* compared to that without salinity.

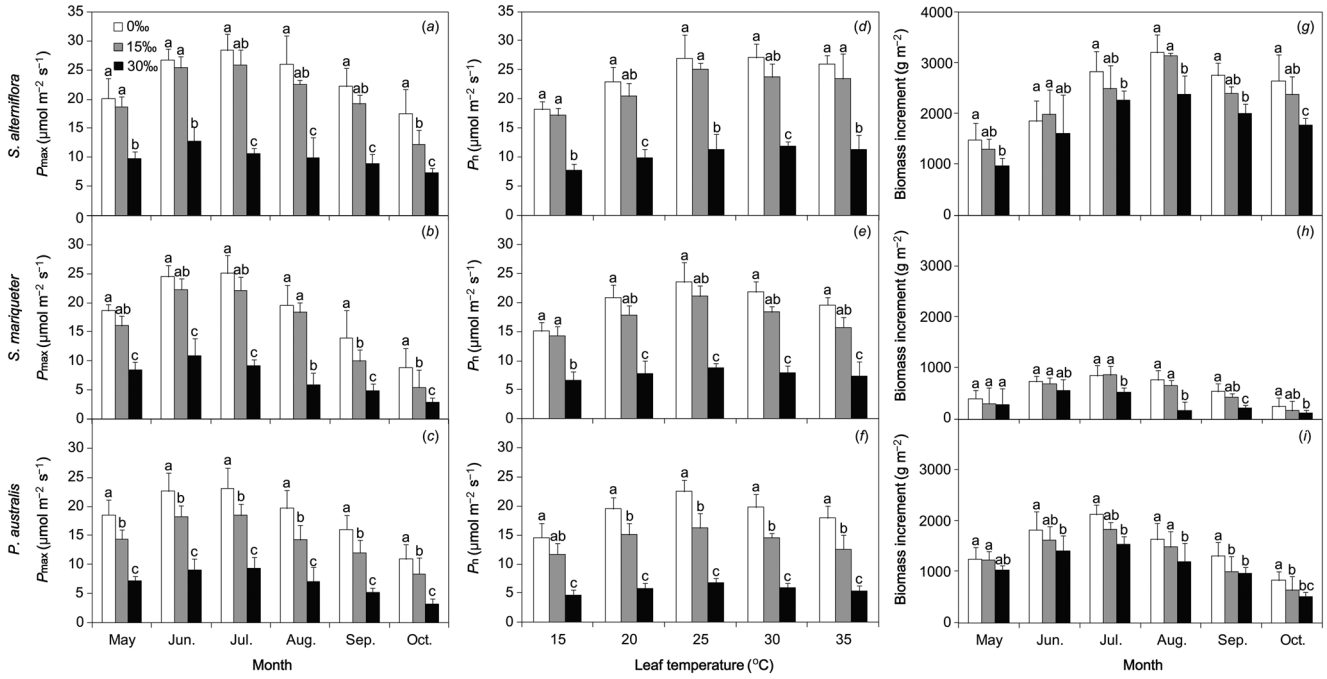

Figure 6. (a–c) Seasonal variations of the maximum net photosynthetic rate (P_{max}), (d–f) the temperature responses of the net photosynthetic rate (P_n), and (g–i) the biomass growth of *S. alterniflora*, *S. mariqueter*, and *P. australis* under different salinity treatments (0‰, 15‰, and 30‰).

Regardless of the species, P_{max} was significantly ($p < 0.05$) reduced under the 30‰ salinity treatment over the growing season. In July, the temperature-dependent photosynthetic rate under varying salinity treatments was investigated for the three species, as presented in Figures 6d–6f. Over the range of measurement temperatures, P_n was reduced by 8.6% and 10.5% ($p > 0.05$), on average, for *S. alterniflora* and *S. mariqueter* under moderate salinity and by 44.8% and 59.2% ($p < 0.05$) under high salinity, respectively, compared with that without salt. P_n in *P. australis* was significantly lower, by 22.1% and 69.8% ($p < 0.05$) under the 15‰ and 30‰ salinity treatments, respectively, over the range of temperatures. There were no significant differences in the annual increment of biomass in the three species between the moderate salinity and no-salt treatments, except for that of *P. australis* at the latter stage (Figures 6g–6i). High-salinity stress significantly ($p < 0.05$) decreased the biomass growth in all species.

3.4. Vegetation Pattern Under SLR and SR

With the species-specific parameterization based on the interaction between biotic and abiotic processes, the vegetation pattern model reproduced the dynamics of the community in the CDW and JW during the period from 2000 to 2008 (Figure 7). The correlations between the modeled area of the three species against the measured values in the corresponding year were high and statistically significant (linear regression, $R^2 = 0.89$–0.97). The model parameterized with the limit of tolerance of *S. alterniflora* revealed that the

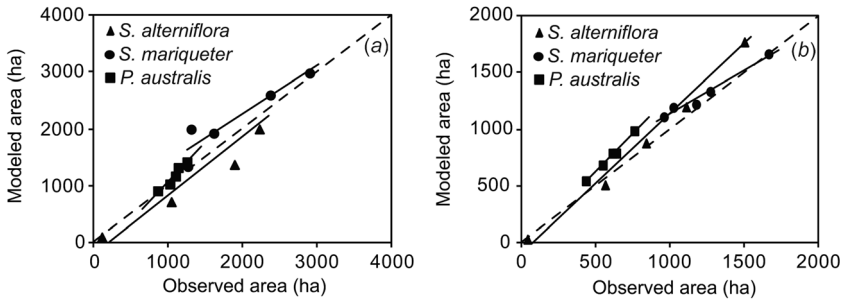

Figure 7. Modeled and observed area of salt marsh vegetation in the (a) CDW and (b) JW after the *S. alterniflora* invasion from 2000 to 2008.

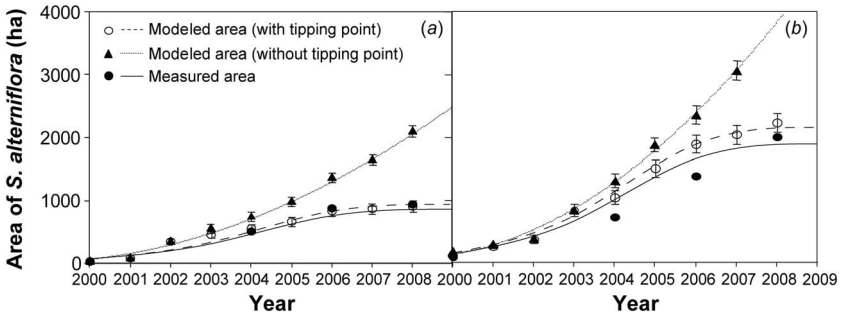

Figure 8. Modeled expansion area of *S. alterniflora* in the (a) CDW and (b) JW during the period 2000–2008, against the observed area. The bars represent the variation over 10 repeated simulations.

expansion rate of this exotic species had slowed down since 2006, after the initial rapid invasion period (Figure 8). If the limit of tolerance under inundation stress was omitted, the expansion rate of the exotic species would be much higher than the current state.

During the simulation period 2008–2100, the vegetation pattern model was parameterized with the tolerance limits for the three species under inundation stress, to assess the degradation thresholds for different species under the SLR and SR scenarios with the result that the vegetation zone located in the high intertidal zone may be degraded into bare mudflats or replaced by other neighboring species (with higher tolerance to inundation). Consequently, the dynamics of the vegetation pattern under the current, SLR and SLR+SR, scenarios in the CDW and JW was predicted from 2008 to 2100, as shown in Figure 9. Regardless of the site and species, the area occupied by vegetation increased under the current scenario over the simulation period (Figure 10). When the scenarios of SLR and SLR+SR were assumed, the area of *S. alterniflora* decreased throughout the simulation period in both the CDW and JW. The area of *P. australis* increased to a peak by approximately 2020 in the CDW and 2045 in the JW, and thereafter, it declined. Under the SLR scenario, the total area (the CDW and JW) of *S. alterniflora* significantly decreased ($p < 0.05$) by approximately 2050 compared with the current scenario (Table 2) and the SLR+SR scenario resulted in a further decrease in the area of *S. alterniflora* and *P. australis* during the latter simulation period.

In contrast, the area of *S. mariqueter* increased to a peak by approximately 2070 (both SLR and SLR+SR) in the CDW and by 2050 (SLR) and 2045 (SLR+SR) in the JW (Figures 10b and 10e). By 2025 and 2050, the total area of *S. mariqueter* under the SLR+SR scenario was significantly ($p < 0.05$) greater than under the current scenario (Table 2). At the end of the simulation period, the area of *S. mariqueter* did not decrease significantly, while the total area of the salt marsh vegetation fell significantly ($p < 0.05$) under the SLR+SR scenario relative to the current scenario.

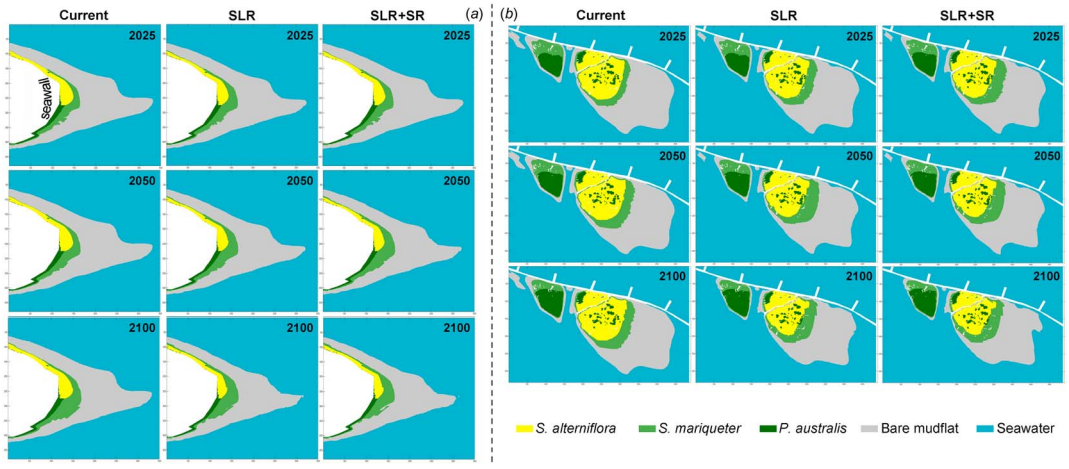

Figure 9. Spatial projections of the vegetation pattern in the (a) CDW and (b) JW in the short term (2025), medium term (2050), and long term (2100) under the current and changed (SLR and SLR+SR) scenarios.

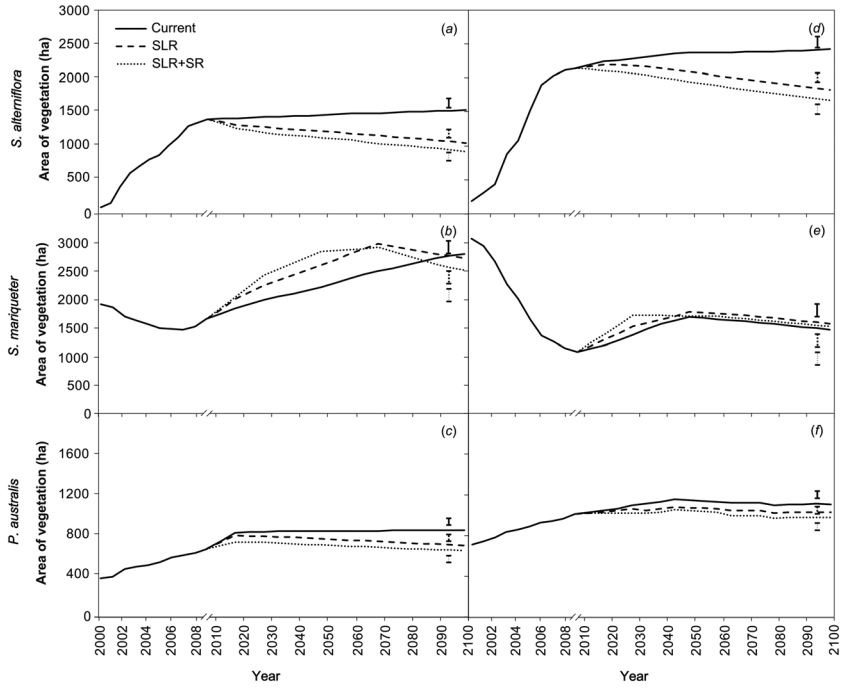

Figure 10. Predicted area of *S. alterniflora*, *S. mariqueter*, and *P. australis* in the (a–c) CDW and (d–f) JW over the simulation period from 2000 to 2100 under the current and changed (SLR and SLR+SR) scenarios. Bars indicate the average standard error ($n = 10$ repeated simulations) over the simulation period.

3.5. Primary Production Under SLR, SR, and SWI

The primary production model, embedded into the vegetation pattern model, simultaneously calculated the variability of GPP under the current, SLR and SLR+SR, SLR+SWI, and SLR+SR+SWI, scenarios (Figure 11). Under the current scenario, the annual amount of GPP (combination of the CDW and JW) of the three species increased over the simulation period. When the SLR and SLR+SR scenarios were assumed, the GPP of *S. alterniflora* decreased over the simulation period, and the decrease was significant ($p < 0.05$) by 2100 when compared with the current scenario (Table 3). The GPP of *S. mariqueter* and *P. australis* increased to a peak by approximately 2060–2070 and 2020–2030, respectively, under the SLR and SLR+SR scenarios, and thereafter, it declined. By 2100, the GPP of *P. australis* was significantly ($p < 0.05$) lower under the SLR+SR scenario than under the current scenario, while the GPP of *S. mariqueter* did not decrease significantly.

Under the SLR+SWI and SLR+SR+SWI scenarios, the GPP of *S. alterniflora* and *P. australis* decreased over the simulation period. The GPP of *S. mariqueter* increased to a peak by approximately 2070 and 2050 under the SLR+SWI and SLR+SR+SWI scenarios, respectively,

Table 2. Percentage Changes (Standard Errors) in the Total Area of Vegetation in the Two Salt Marshes (the CDW and JW) Under the SLR and SLR+SR Scenarios Compared to the Current Scenario by 2025, 2050, and 2100

	Scenario	
Vegetation	SLR	SLR+SR
	2025	
S. alterniflora	−5.4(0.1)	−10.1(0.3)
S. mariqueter	8.3(0.2)	16.1(0.5)[a]
P. australis	−2.7(0.0)	−7.5(0.2)
Total	−1.0(0.0)	−1.2(0.0)
	2050	
S. alterniflora	−13.7(0.4)	−20.4(0.8)[b]
S. mariqueter	12.3(0.3)	16.7(0.6)[a]
P. australis	−7.4(0.2)	−12.2(0.3)
Total	−1.9(0.0)	−3.8(0.0)
	2100	
S. alterniflora	−28.1(0.7)[b]	−35.0(1.1)[b]
S. mariqueter	0.5(0.0)	−5.7(0.1)
P. australis	−12.1(0.3)	−17.3(0.5)[a]
Total	−13.0(0.4)	−19.3(0.6)[b]

[a] $p < 0.05$.
[b] $p < 0.01$.

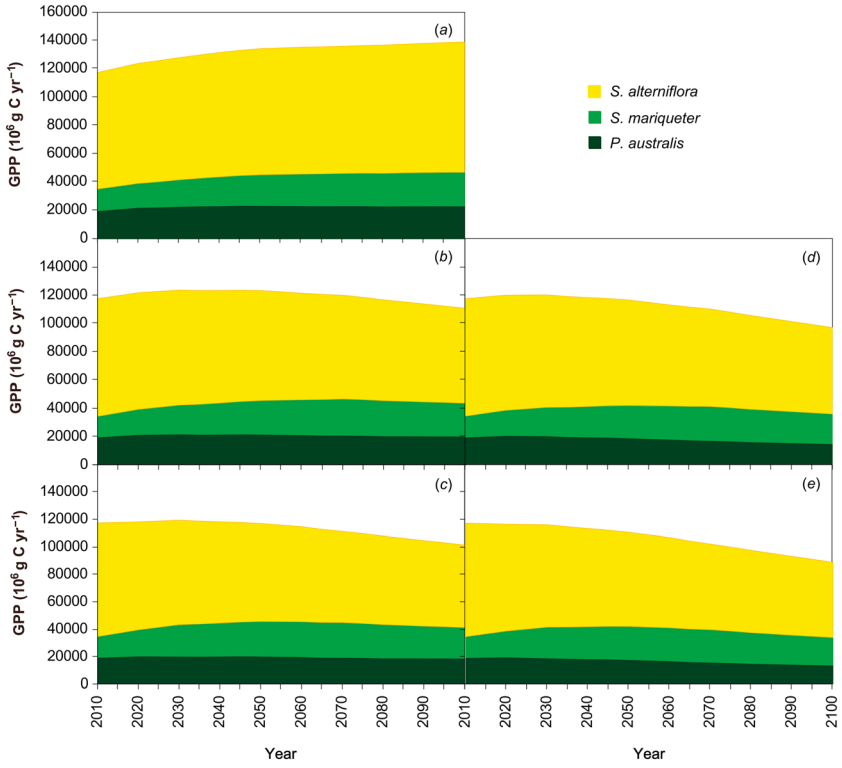

Figure 11. Predicted gross primary production (GPP, combination of the CDW and JW) of *S. alterniflora*, *S. mariqueter*, and *P. australis* over the simulation period from 2010 to 2100 under the (a) current and (b–e) changed (SLR, SLR+SR, SLR+SWI, and SLR+SR+SWI) scenarios.

and thereafter, it declined. The SLR+SWI and SLR+SR+SWI scenarios resulted in significant ($p < 0.05$) decreases in the GPP of *S. alterniflora* and *P. australis* starting by approximately 2050 when compared with the current scenario, and this occurred during the latter simulation period for *S. mariqueter* (Table 3). By 2100, total GPP of all three species was significantly ($p < 0.05$) lower than the current scenario, regardless

Table 3. Percentage Changes (Standard Errors) in the Gross Primary Production (GPP) of Vegetation in the Two Salt Marshes (the CDW and JW) Under the SLR, SLR+SR, SLR+SWI, and SLR+SR+SWI Scenarios Compared to the Current Scenario by 2025, 2050, and 2100

	Scenario			
Vegetation	SLR	SLR+SR	SLR+SWI	SLR+SR+SWI
		2025		
S. alterniflora	−5.7(0.1)	−10.8(0.3)	−6.7(0.1)	−11.4(0.2)
S. mariqueter	7.9(0.1)	15.5(0.4)[a]	8.4(0.2)	16.0(0.5)[a]
P. australis	−3.2(0.0)	−8.0(0.1)	−6.8(0.1)	−11.4(0.2)
Total	−2.7(0.0)	−5.6(0.1)	−4.6(0.0)	−7.5(0.1)
		2050		
S. alterniflora	−14.1(0.4)	−20.6(0.9)[b]	−17.1(0.4)[a]	−23.5(0.9)[b]
S. mariqueter	11.5(0.3)	16.2(0.6)[a]	7.4(0.2)	11.5(0.2)
P. australis	−8.2(0.1)	−12.8(0.3)	−18.1(0.4)[a]	−22.4(0.6)[b]
Total	−8.4(0.2)	−13.0(0.4)	−13.3(0.3)	−17.6(0.4)[a]
		2100		
S. alterniflora	−28.5(0.7)[b]	−35.7(1.0)[b]	−34.3(0.9)[b]	−40.7(1.4)[b]
S. mariqueter	0.3(0.0)	−6.1(0.1)	−9.6(0.2)	−15.1(0.5)[a]
P. australis	−12.4(0.3)	−17.9(0.2)[a]	−35.2(1.0)[b]	−39.0(1.2)[b]
Total	−20.5(0.6)[b]	−27.0(0.6)[b]	−30.2(0.8)[b]	−36.0(0.7)[b]

[a] $p < 0.05$;
[b] $p < 0.01$

of the changed scenarios. Over the simulation period, the mean values of the GPP amount were reduced by 9.8% under SLR, 16.0% under SLR+SR, 17.8% under SLR+SWI, and 22.9% under SLR+SR+SWI when compared to the current scenario.

4. Discussion

4.1. Impacts of Environmental Change

China's coastline extends for approximately 18,000 km, in which coastal wetlands, with a total area of ~5.8×10^4 km^2, provide important ecosystem services [*Guan*, 2012]. However, combinations of rise in sea level, reduced sediments, and colonization of exotic species, with the disturbance of human activity and river flow, will cause a great impact on vegetation community and its ecological functions such as primary production [*Chen et al*., 2008; *Guan*, 2012].

On China's coastline, the rapid expansion of *S. alterniflora* occurred because of the high availability of suitable habitat during the initial introduction period. Historical survey has indicated that the rapid invasion of *S. alterniflora* could largely be attributed to a greater distance of seedling dispersal, a larger seed bank, and a higher survival rate of its propagules relative to the two dominant native species [*Xiao et al*., 2009, 2010; *Ge et al*., 2013, 2015a]. Previous studies also demonstrated that *S. alterniflora* could quickly invade unvegetated zones and the habitat of *S. mariqueter* [*Chen et al*., 2004; *Wang et al*., 2006; *Li et al*., 2009]. The dominant native species *S. mariqueter* and *P. australis* colonized new habitats at a slower rate, mainly through underground asexual colonization. With the species-specific parameterization in terms of the interaction between biotic and abiotic processes [*Ge et al*., 2013, 2015a], the vegetation model was able to reproduce the community dynamics after the initial introduction of *S. alterniflora* in the two largest coastal wetlands in the Yangtze Estuary during the period 2000 to 2008.

However, both the current fixed-point field monitoring and inundation experiments revealed that the tolerance limits for the survival of *S. alterniflora* (and also *P. australis*) were lower than that of *S. mariqueter*. This suggested that in the coastal area, the pioneer Cyperaceae species showed greater tolerance under prolonged inundation relative to the exotic Poaceae. The range expansion of both exotic and native species is dependent on the accretion rate of intertidal mudflats (newly formed habitat). The model indicated that the expansion rate of *S. alterniflora* slowed down until 2100 under the current scenario, suggesting that the current sedimentation rate may not support the high-speed expansion of *S. alterniflora* due to the decreasing availability of the habitat for establishment [*Ge et al*., 2015a]. *Zhang et al*. [2004] also found that annual mean expansion rate of *S. alterniflora* decreased to less than 10% after a rapid invasion period along the coast of Jiangsu Province (31°N–35°N).

As documented by *SOA* [2013], the rate of SLR in China was higher than the global average level. On the other hand, China's coastal wetlands have been enclosed by thousands of kilometers of seawalls because of planning for economic growth, especially in East China [*Ma et al*., 2014]. The effect of this "coastal squeeze," whereby change in the area of salt marsh is greatly restricted, is to seriously weaken the potential adaptability of coastal ecosystems to SLR, specifically inland migration [*Feagin et al*., 2010; *Mendoza-González et al*., 2013]. As a result, coastal plants are directly exposed to the risk of SLR and SR and a consequent change in geographical features and saltwater intrusion. Under the SLR scenario, the vegetation pattern model predicted that the colonization of *S. alterniflora* and the native *P. australis* would be limited. In the Yangtze Estuary, the large amount of hydraulic engineering (including TGD) upstream on the Yangtze River has decreased the sediment discharge, leading to a continuous reduction in the sedimentation rate in the Yangtze Estuary [*Yang et al*., 2011]. As a result, the SLR+SR scenario led to further degradation. Many studies had reported that environmental change would allow an increase in invader dominance by favoring those species that are more tolerant of altered conditions [*Thuiller et al*., 2007; *Mason et al*., 2012; *Sheppard et al*., 2014], but some researchers had assumed that environmental change may reduce the competitiveness of invasive plants if conditions become climatically unsuitable [*Bradley et al*., 2009]. The situation as described here in the coastal habitats of the Yangtze Estuary corresponds to the findings of *Dostál et al*. [2013], who indicated that the initial dominance of invasive species can later be reversed by stabilizing processes.

In the Yangtze Estuary, the area of *S. mariqueter* would increase due to less stress from *S. alterniflora* after 2006–2008. *S. mariqueter* might also recolonize the invaded habitat by *S. alterniflora*, resulting in increases

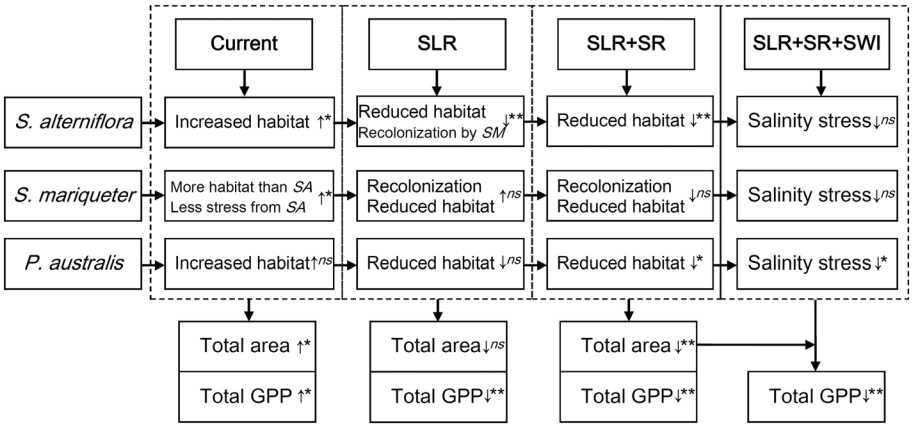

Figure 12. Analysis of changes in the pattern vegetation and primary production in the coastal wetlands under the current and changed scenarios.

in its area, with a higher recolonization rate during the latter simulation period (Figure 12). As observed in the field, *S. mariqueter* can expand continuously in low-lying habitats, even in seaward eroded mudflats (see Figure 13). *Mendoza-González et al.* [2013] also reported that this endemic species might be specifically adapted to the salt marsh environment in Chinese coastal ecosystems. In this study, the single scenario of SLR did not reduce the total area of wetland vegetation significantly due to the mitigating effects of sediment accretion and the resilience of *S. mariqueter* in the Yangtze Estuary. Another native species, *P. australis*, which is mostly located in the high-elevation habitat, would expand continuously but at a low rate. On the other hand, the model was parameterized with the capability of salt marsh vegetation to trap suspended sediment, and the positive feedback loop between vegetation expansion and sediment deposition probably favors the self-regulation of salt marshes and resilience to SLR. However, the potential risk of prolonged flooding became exacerbated under the combined scenario of SLR+SR, probably resulting in a significant degradation of the coastal wetlands. In addition to the response of plant survival, the seed setting rates (data not presented) of all species were substantially decreased under inundation stress, which might affect the colonization of vegetation negatively in subsequent generations.

The second aim of this study was to assess the impact of SLR, SR, and SWI on the primary production of wetland vegetation. For this purpose, a detailed process-based primary production model with the incorporation of photosynthetic parameters under a salinity gradient [*Ge et al.*, 2014, 2015b] was embedded into the vegetation pattern model. Under the conditions of SLR and SR, the loss of vegetation was shown to result in an immediate reduction in GPP. Salinity stress is another environmental factor that was taken into consideration because *Qiu and Zhu* [2015] and *Yuan et al.* [2015] demonstrated that SLR may increase the salt supply. Based on the prediction of the coupled model, the SWI scenario would exacerbate the impacts of SLR and SR on the total primary production of the salt marsh vegetation, especially *P. australis* (Figure 12).

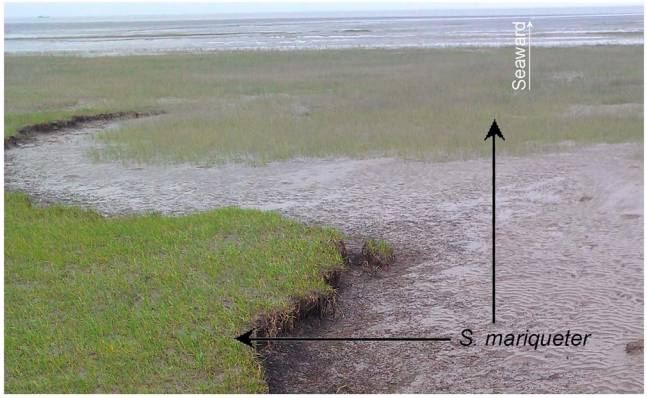

Figure 13. Colonization of *S. mariqueter* in low-lying seaward habitat (photo by Ge Z.M.).

Based on the salinity stress experiments, the photosynthetic performance of *S. alterniflora* and *S. mariqueter* was not significantly limited under a moderate salinity level. This suggested a greater salt tolerance of the exotic C_4 plant and the native Cyperaceae. Generally, C_4 plants have higher assimilation rates of CO_2, and this contributes to their salt tolerance by reducing the amount of water

and therefore salt that the roots must process to support growth [*Flowers et al*., 1977]. *S. alterniflora* was able to use nitrogen ions for osmotic adjustments in its shoots, avoiding salinity stress [*Vasquez et al*., 2006]. Previous measurements also found that the photosynthetic parameters of the maximum rate of carboxylation by Rubisco, the maximum rate of electron transport, and the maximum rate of PEP carboxylation showed a lower sensitivity to moderate stress [*Ge et al*., 2014]. The greater tolerance of *S. mariqueter* under moderate salinity may be attributed to its leaf morphology (prismatic shape) and physiological constraints in terms of water conservation [*Hester et al*., 2001; *Jiang et al*., 2009], which also indicated that *S. mariqueter* could adapt to the habitat conditions at a very low elevation. The photosynthetic rate, as well as the biochemical parameters of *P. australis*, decreased significantly, regardless of stress levels, confirming that salinity is a well-known stressor of *P. australis* [*Burdick et al*., 2001; *Vasquez et al*., 2006; *Ge et al*., 2015a]. This might partly explain why most *P. australis* grows in the high-elevation habitat, where there is lower stress [*Mauchamp and Mésleard*, 2001].

In this simulation study, a moderate scenario (increase to 10‰) was assumed. Although many species are tolerant to moderate salinity during the growth stages of seed setting and germination, most studies have indicated that plants are particularly susceptible to salinity during the seedling and early vegetative growth stage compared with the germination stage [*Läuchli and Grattan*, 2007]. As expected, an extended duration of saltwater intrusion might thus result in serious degradation of the coastal ecosystems in East China by limiting the growth and survival of both exotic and native vegetation throughout their life cycles.

4.2. Uncertainty Analysis

This study focused on stress experiments and a modeling exercise to understand the spatiotemporal dynamics of vegetation community and primary production (exotic and native species) facing risks of SLR, SR, and SWI in coastal areas. However, there are several issues with the model construction and prediction linked to uncertainty. The model used historic records of the sedimentation rate but did not include a marsh accretion module. The sediment deposition rates in the marsh are largely controlled by the duration and frequency of tidal inundation [*Marion et al*., 2009]. Therefore, potential changes in sediment loading and tidal flooding after SLR may lead to uncertainty in the accretion estimates. The tolerance threshold of exotic and native species to inundation stress is one of the core features of the model. The wetland plants may show greater morphological plasticity in response to inundation [*Kirwan and Guntenspergen*, 2012]. The sensitivity analysis (±15% at species tolerance levels) showed that the model outputs were sensitive (variation of $-8\% \pm 12\%$) to changes in the species-specific tolerance thresholds to submergence. Thus, the findings on the effects of SLR and SR on the pattern of vegetation should be reasonable, based on the detailed parameterization of species-specific biotic processes.

Regarding the experimental design, the field trial for testing the synergetic stress of inundation and salinity was not conducted for model calibration and validation, probably leading to an underestimation of the impact of SLR+SWI on seed/seedling production, vegetation expansion, and establishment. Another issue is that the model ignored the spatial heterogeneity of primary production in vegetation growing along the tidal level gradient. Related studies have found that the biomass and productivity of salt marsh macrophytes varies strongly with tidal amplitude, sediment supply, and marsh elevation [*Morris et al*., 2002; *Fagherazzi et al*., 2012; *Kirwan and Guntenspergen*, 2012]. In addition, SLR and extreme weather events may induce changes in primary production in the coastal wetland through lateral flow or through decreasing the quantity of sediments [*Yan et al*., 2008]. Therefore, more work on the field trial and model updating for the coastal ecosystems is needed.

On the other hand, there are still uncertainties associated with human influence. For instance, a huge damming project has been in process in the CDW in order to eradicate the exotic species. Upon the completion of the project, the distribution of *S. alterniflora* might not match the model predictions for further vegetation patterns and figures for primary production.

5. Conclusions

This study explored the future vegetation patterns and primary production in coastal areas under the scenarios of SLR, SR, and SWI. Although historical surveys had indicated a rapid expansion of exotic species, both the current monitoring and inundation stress experiments revealed that *S. mariqueter* has a greater tolerance under prolonged inundation relative to *S. alterniflora* and *P. australis*. As a result, the vegetation pattern

model predicted that the expansion rate of exotic species would slow down by the end of the simulation period under the current scenario and that the SLR scenario might limit the colonization of *S. alterniflora* and *P. australis*. In contrast, the area of *S. mariqueter* would increase due to less competitive stress from *S. alterniflora* in the low-lying habitats and even recolonize invaded areas under the SLR scenario. The SLR+SR scenario would result in the further degradation of coastal wetlands while not significantly reducing the area of *S. mariqueter*. The embedded primary production model predicted that the decrease in vegetation area would directly reduce the total GPP under the SLR and SR conditions. The SWI scenario would exacerbate the impacts of SLR and SR on GPP, especially for *P. australis*, because the stress experiments revealed that *S. alterniflora* and *S. mariqueter* have a higher tolerance for moderate salinity relative to *P. australis*. With the coastal squeeze effects from the construction of massive seawalls in China, the inland migration of vegetation is hindered. Accordingly, this research indicated that the coastal vegetation pattern would be modified significantly due to a recovery opportunity for the native *S. mariqueter* and the simultaneous potential for degradation of the exotic species *S. alterniflora* following changed geophysical features, especially with coastal squeeze. This study also showed that the native species that are better adapted to prolonged inundation and increased salinity might become key contributors to primary production on the muddy coasts of East China.

Acknowledgments

This work was supported by the National Natural Science Foundation of China (41571083, 41271065 and 41201091), the Marine Science Project (14DZ1206004) of Shanghai Science and Technology Committee, and the autonomous research fund of the SKLEC. The data for this paper are available, and Z.M. Ge (zmge@sklec.ecnu.edu.cn) can be contacted for access to the data. We thank Martin Kent (Plymouth University, UK) for kindly editing the language and assisting with the revision of the original manuscript.

References

Bradley, B. A., M. Oppenheimer, and D. S. Wilcove (2009), Climate change and plant invasions: Restoration opportunities ahead?, *Global Change Biol.*, *15*, 1511–1521.

Burdick, D. M., R. Buchsbaum, and E. Holt (2001), Variation in soil salinity associated with expansion of *Phragmites australis* in salt marshes, *Environ. Exp. Bot.*, *46*, 247–261.

Chen, J., B. Zhao, W. Ren, S. C. Saunders, Z. Ma, B. Li, Y. Luo, and J. Chen (2008), Invasive *Spartina* and reduced sediments: Shanghai's dangerous silver bullet, *J. Plant Ecol.*, *1*, 79–84.

Chen, Z. Y., B. Li, Y. Zhong, and J. K. Chen (2004), Local competitive effects of introduced *Spartina alterniflora* on *Scirpus mariqueter* at Dongtan of Chongming Island, the Yangtze River estuary and their potential ecological consequences, *Hydrobiologia*, *528*, 99–106.

Church, J. A., et al. (2013), in *Sea Level Change. In: Climate Change 2013: The Physical Science Basis. Contribution of Working Group I to the Fifth Assessment Report of the Intergovernmental Panel on Climate Change*, edited by T. F. Stocker et al., Cambridge Univ. Press, Cambridge, U. K., and New York.

Conrads, P. A., E. A. Roehl, R. C. Daamen, and J. B. Cook (2013), Simulation of salinity intrusion along the Georgia and South Carolina coasts using climate-change scenarios, *U.S. Geol. Surv. Sci. Invest. Rep.*, 92 pp.

Changjiang Water Resources Commission (2012), *Changjiang Sediment Bulletin*, 40 pp., Changjiang Press, Hubei, Wuhan, China.

Dostál, P., J. Müllerová, P. Pyšek, J. Pergl, and T. Klinerová (2013), The impact of an invasive plant changes over time, *Ecol. Lett.*, *16*, 1277–1284.

Fagherazzi, S., et al. (2012), Numerical models of salt marsh evolution: Ecological, geomorphic, and climatic factors, *Rev. Geophys.*, *50*, RG1002, doi:10.1029/2011RG000359.

Farquhar, G. D., S. von Caemmerer, and J. A. Berry (2001), Models of photosynthesis, *Plant Physiol.*, *125*, 42–45.

Feagin, R. A., M. L. Martínez, G. Mendoza-González, and R. Costanza (2010), Salt marsh zonal migration and ecosystem service change in response to global sea level rise: A case study from an urban region, *Ecol. Soc.*, *15*, 14.

Flowers, T. J., P. F. Troke, and A. R. Yeo (1977), The mechanism of salt tolerance in halophytes, *Annu. Rev. Plant Physiol.*, *28*, 89–121.

Ge, Z. M., T. H. Wang, K. Y. Wang, and X. M. Wang (2008), *Characteristics of Coastal Wetland Ecosystem of the Yangtze Estuary and Conservation for Key Communities*, 189 pp., Science Press, Beijing.

Ge, Z. M., X. Zhou, S. Kellomäki, H. Peltola, and K. Y. Wang (2012), Measured and modeled biomass growth in relation to photosynthesis acclimation of a bioenergy crop (Reed canary grass) under elevated temperature, CO_2 enrichment and different water regimes, *Biomass Bioenerg.*, *46*, 251–262.

Ge, Z. M., H. B. Cao, and L. Q. Zhang (2013), A process-based grid model for the simulation of range expansion of *Spartina alterniflora* on the coastal saltmarshes in the Yangtze Estuary, *Ecol. Eng.*, *58*, 105–112.

Ge, Z. M., L. Q. Zhang, L. Yuan, and C. Zhang (2014), Effects of salinity on temperature-dependent photosynthetic parameters of a native C_3 and a non-native C_4 marsh grass in the Yangtze Estuary, China, *Photosynthetica*, *52*, 484–492.

Ge, Z. M., L. Q. Zhang, and L. Yuan (2015a), Spatiotemporal dynamics of salt marsh vegetation regulated by plant invasion and abiotic processes in the Yangtze Estuary: Observations with a modeling approach, *Estuarine Coastal Shelf Sci.*, *38*, 310–324.

Ge, Z. M., H. Q. Guo, B. Zhao, and L. Q. Zhang (2015b), Plant invasion impacts on the gross and net primary production of the salt marsh on eastern coast of China: Insights from leaf to ecosystem, *J. Geophys. Res. Biogeosci.*, *120*, 169–186, doi:10.1002/2014JG002736.

Guan, D. M. (2012), *China's Coastal Wetlands*, pp. 233, Science Press, Beijing.

Hester, M. W., I. A. Mendelssohn, and K. L. McKee (2001), Species and population variation to salinity stress in Panicum hemitomon, Spartina patens, and Spartina alterniflora: Morphological and physiological constraints, *Environ. Exp. Bot.*, *46*, 277–297.

Jiang, L. F., Y. Q. Luo, J. K. Chen, and B. Li (2009), Ecophysiological characteristics of invasive *Spartina alterniflora* and native species in salt marshes of Yangtze River estuary, China, *Estuarine Coastal Shelf Sci.*, *81*, 74–82.

Kirwan, M. L., and G. R. Guntenspergen (2012), Feedbacks between inundation, root production, and shoot growth in a rapidly submerging brackish marsh, *J. Ecol.*, *100*, 764–770.

Kong, Y. Z., S. L. He, P. X. Ding, and K. L. Hu (2004), Characteristics of temporal and spatial variation of salinity and their indicating significance in the Changjiang Estuary, *Acta. Oceanol. Sin.*, *26*, 9–18.

Läuchli, A., and S. R. Grattan (2007), Plant growth and development under salinity stress, in *Advances in Molecular Breeding Toward Drought and Salt Tolerant Crops*, edited by M. Jenls, P. M. Hasegawa, and S. M. Jain, pp. 1–32, Springer, Netherlands.

Li, B., et al. (2009), *Spartina alterniflora* invasions in the Yangtze River estuary, China: An overview of current status and ecosystem effects, *Ecol. Eng.*, *35*, 511–520.

Ma, Z. J., X. J. Gan, Y. T. Cai, J. K. Chen, and B. Li (2011), Effects of exotic Spartina alterniflora on the habitat patch associations of breeding saltmarsh birds at Chongming Dongtan in the Yangtze River estuary, China, *Biol. Invasions*, *13*, 1673–1686.

Ma, Z. J., D. S. Melville, J. G. Liu, Y. Chen, H. Y. Yang, W. W. Ren, Z. W. Zhang, T. Piersma, and B. Li (2014), Rethinking China's new great wall, *Science*, *346*, 912–914.

Marion, C., E. J. Anthony, and A. Trentesaux (2009), Short-term estuarine mudflat and saltmarsh sedimentation: High-resolution data from ultrasonic altimetry, rod surface elevation table, and filter traps, *Estuarine Coastal Shelf Sci.*, *83*, 475–484.

Mason, T. J., K. French, and K. Russell (2012), Are competitive effects of native species on an invader mediated by water availability?, *J. Veg. Sci.*, *23*, 657–666.

Mauchamp, A., and F. Mésleard (2001), Salt tolerance in *Phragmites australis* populations from coastal Mediterranean marshes, *Aquat. Bot.*, *70*, 39–52.

Mendoza-González, G., M. L. Martínez, D. Martínez-Gordillo, O. R. Rojas-Soto, G. Vázquez, and J. B. Gallego-Fernández (2013), Environmental niche modeling of coastal dune plants and its future potential distribution in response to climate change and sea level rise, *Global Change Biol.*, *19*, 2524–2535.

Morris, J. T., P. V. Sundareshwar, C. T. Nietch, B. Kjerfve, and D. R. Cahoon (2002), Responses of coastal wetlands to rising sea level, *Ecology*, *83*, 2869–2877.

Mudd, S. M., S. M. Howell, and J. T. Morris (2009), Impact of dynamic feedbacks between sedimentation, sea-level rise, and biomass production on near-surface marsh stratigraphy and carbon accumulation, *Estuarine Coastal Shelf Sci.*, *82*, 377–389.

Qiu, C., and J. R. Zhu (2015), Assessing the influence of sea level rise on salt transport processes and estuarine circulation in the Changjiang River estuary, *J. Coastal Res.*, *31*, 661–670.

Schwarz, C., T. Ysebaert, Z. C. Zhu, L. Q. Zhang, T. J. Bouma, and P. M. J. Herman (2011), Abiotics governing the establishment and expansion of two contrasting salt marsh species in the Yangtze Estuary, China, *Wetlands*, *31*, 1011–1021.

Scott, R. L., E. P. Hamerlynck, G. D. Jenerette, M. S. Moran, and G. A. Barron-Gaffors (2010), Carbon dioxide exchange in a semidesert grassland through drought-induced vegetation change, *J. Geophys. Res.*, *115*, G03026, doi:10.1029/2010JG001348.

Seabloom, E. W., P. Ruggiero, S. D. Hacker, J. Mull, and P. Zarnetske (2013), Invasive grasses, climate change, and exposure to storm-wave overtopping in coastal dune ecosystems, *Global Change Biol.*, *19*, 824–832.

Sheppard, C. S., B. R. Burns, and M. C. Stanley (2014), Predicting plant invasions under climate change: Are species distribution models validated by field trials?, *Global Change Biol.*, *20*, 2800–2814.

State Oceanic Administration People's Republic of China (SOA) (2013), Bulletin of Chinese sea level rise. [Available at http://www.coi.gov.cn/gongbao/nrhaipingmian/nr2013/201403/t20140317_30622.html.]

Thuiller, W., D. W. Richardson, and G. F. Midgley (2007), Will climate change promote alien plant invasions?, in *Biological Invasions*, edited by W. Nentwig, pp. 197–211, Springer, Berlin.

Vasquez, E. A., E. P. Glenn, G. R. Guntenspergen, J. J. Brown, and S. G. Nelson (2006), Salt tolerance and osmotic adjustment of *Spartina alterniflora* (Poaceae) and the invasive M haplotype of *Phragmites australis* (Poaceae) along a salinity gradient, *Am. J. Bot.*, *93*, 1784–90.

von Caemmerer, S., and R. T. Furbank (1999), Modeling C_4 photosynthesis, in *C_4 Plant Biology*, edited by R. F. Sage and R. K. Monson, pp. 173–211, Acad. Press, Toronto, Ontario, Canada.

Wang, H., Z. M. Ge, L. Yuan, and L. Q. Zhang (2014), Evaluation of the combined threat from sea-level rise and sedimentation reduction to the coastal wetlands in the Yangtze Estuary, China, *Ecol. Eng.*, *71*, 346–354.

Wang, Q., C. H. Wang, B. Zhao, Z. J. Ma, Y. Q. Luo, J. K. Chen, and B. Li (2006), Effects of growing conditions on the growth and interactions between salt marsh plants: Implications for invasibility of habitats, *Biol Invasions*, *8*, 1547–1560.

Xiao, D. R., L. Q. Zhang, and Z. C. Zhu (2009), A study on seed characteristics and seed bank of *Spartina alterniflora* at saltmarshes in the Yangtze Estuary, China, *Estuarine Coastal Shelf Sci.*, *83*, 105–110.

Xiao, D. R., L. Q. Zhang, and Z. C. Zhu (2010), The range expansion patterns of *Spartina alterniflora* on saltmarshes in the Yangtze Estuary, China, *Estuarine Coastal Shelf Sci.*, *88*, 99–104.

Yan, Y. E., B. Zhao, J. Q. Chen, H. Q. Guo, Y. J. Gu, Q. H. Wu, and B. Li (2008), Closing the carbon budget of estuarine wetlands with tower-based measurements and MODIS time series, *Global Change Biol.*, *14*, 1690–1702.

Yang, S. L., J. Zhang, J. Zhu, J. P. Smith, S. B. Dai, and A. Gao (2005), Impact of dams on Yangtze River sediment supply to the sea and delta wetland response, *J. Geophys. Res.*, *110*, F03006, doi:10.1029/2004JF000271.

Yang, S. L., J. D. Milliman, P. Li, and K. Xu (2011), 50,000 dams later: Erosion of the Yangtze River and its delta, *Global Planet. Change*, *75*, 14–20.

Yuan, R., J. R. Zhu, and B. Wang (2015), Impact of sea-level rise on saltwater intrusion in the Pearl River Estuary, *J. Coastal Res.*, *31*, 477–48.

Zhang, R. S., Y. M. Shen, L. Y. Lu, S. G. Yan, Y. H. Wang, J. L. Li, and Z. L. Zhang (2004), Formation of *Spartina alterniflora* salt marshes on the coast of Jiangsu Province, China, *Ecol. Eng.*, *23*, 95–105.

Zhou, Y. X., and Y. M. Xie (2012), *Study on Wetlands Resource Investigation and Monitoring and Evaluation System*, 152 pp., Shanghai Sci. and Technol. Press, Shanghai, China.